Tracking brain states under general anesthesia by using global coherence analysis

Aylin Cimenser[a,b,c,1], Patrick L. Purdon[a,b,c], Eric T. Pierce[a,b], John L. Walsh[a,b], Andres F. Salazar-Gomez[a,c], Priscilla G. Harrell[a,b], Casie Tavares-Stoeckel[a], Kathleen Habeeb[a], and Emery N. Brown[a,b,c,d]

[a]Department of Anesthesia, Critical Care and Pain Medicine, Massachusetts General Hospital, Boston, MA 02114; [b]Harvard Medical School, Boston, MA 02115; and [c]Department of Brain and Cognitive Science and [d]Harvard-MIT Division of Health Sciences and Technology, Massachusetts Institute of Technology, Cambridge, MA 02139

Edited by Rob Kass, Carnegie Mellon University, Pittsburgh, PA, and accepted by the Editorial Board March 25, 2011 (received for review November 12, 2010)

Time and frequency domain analyses of scalp EEG recordings are widely used to track changes in brain states under general anesthesia. Although these analyses have suggested that different spatial patterns are associated with changes in the state of general anesthesia, the extent to which these patterns are spatially coordinated has not been systematically characterized. Global coherence, the ratio of the largest eigenvalue to the sum of the eigenvalues of the cross-spectral matrix at a given frequency and time, has been used to analyze the spatiotemporal dynamics of multivariate time-series. Using 64-lead EEG recorded from human subjects receiving computer-controlled infusions of the anesthetic propofol, we used surface Laplacian referencing combined with spectral and global coherence analyses to track the spatiotemporal dynamics of the brain's anesthetic state. During unconsciousness the spectrograms in the frontal leads showed increasing α (8–12 Hz) and δ power (0–4 Hz) and in the occipital leads δ power greater than α power. The global coherence detected strong coordinated α activity in the occipital leads in the awake state that shifted to the frontal leads during unconsciousness. It revealed a lack of coordinated δ activity during both the awake and unconscious states. Although strong frontal power during general anesthesia-induced unconsciousness—termed anteriorization—is well known, its possible association with strong α range global coherence suggests highly coordinated spatial activity. Our findings suggest that combined spectral and global coherence analyses may offer a new approach to tracking brain states under general anesthesia.

alpha rhythm | delta rhythm | loss of consciousness

Time-domain and frequency displays of continuous surface EEG recordings have been used for many years to track changes in the state of the brain under general anesthesia (1–7). Although these analyses have shown that different spatial patterns appear over the scalp as the state of general anesthesia changes, the extent to which these patterns are spatially coordinated and may indicate interesting dynamics in the underlying brain networks has not been systematically characterized. Several experimental and analysis issues must be addressed to carry out this characterization. First, analysis of this coordinated activity with an appropriate level of spatial resolution requires use of high-density (≥64 leads) EEG recordings (8). With few exceptions, EEG studies of general anesthesia use no more than 20 electrodes (9). Second, although in principle high-density EEG recordings should provide higher resolution information about the spatial structure in brain activity under general anesthesia, the increased amount of data creates the analysis challenge of determining how to make informative temporal assessments of the spatial dynamics in these multivariate time-series. Analyzing the cross-spectral matrix for a range of relevant frequencies as a function of time would offer a way to conduct a temporal analysis of coordinated spatial activity in the brain under general anesthesia.

Third, the cross-spectral matrix is a multivariate quantity at each frequency and therefore requires an informative summary to make its use practical. An accepted practice for summarizing the information in the cross-spectral matrix is to compute the global coherence defined as either the ratio of the largest eigenvalue of this matrix to the sum of the eigenvalues (10), or the average of all of the pairwise coherences (11). Finally, when computing coherence or cross-spectra from multivariate EEG recordings, the choice of the referencing scheme requires careful consideration. An EEG montage in which all of the electrodes are referenced with respect to a single location or to a common average can give the appearance of coordinated activity when in fact little or none is present (12). Local average referencing at each electrode site is a reliable way to distinguish spatial differences in EEG activity and avoid spurious findings of coordinated activity (8). In a simple surface Laplacian reference scheme, each electrode is referenced with respect to an average computed from the electrodes in a local neighbor. Moreover, for a sufficiently dense EEG montage, surface Laplacian referencing provides at each electrode site an approximation to the radial current density (i.e., the currents traveling perpendicular to the scalp).

Global coherence analyses, computed using the eigenvalue definition (10), have been applied to study coordinated activity in multivariate time-series in climatology, optical imaging, functional magnetic resonance imaging, and magnetoencephalography (13–15). Eigenvalue and eigenvector decompositions of cross-spectral matrices computed from EEG recordings with fewer than 32 leads have been used to study spatial dynamics in brain activity during sleep–wake cycles and epilepsy (16–18). To date, these approaches have not been used to analyze the spatiotemporal structure in EEG recorded across different levels of general anesthesia. Using high-density EEG time-series recorded from three human subjects during induction of loss of consciousness by a computer-controlled infusion of the anesthetic propofol, we estimated the radial current density at each electrode site by surface Laplacian scheme and used spectral and eigenvalue-based global coherence analyses to track the spatiotemporal dynamics of the brain's anesthetic state. We show that during unconsciousness the spectrograms of the radial current densities have an increase in α (8–12 Hz) and δ (0–4 Hz) activity in the frontal sites and a decrease in α activity and an increase in δ activity in the occipital sites. The global coherence analysis detects strong coordinated α activity in the occipital sites when the subjects are awake that shifts to the frontal sites when the subjects are unconscious. Global coherence is not strong in the δ range during either the awake or the unconscious state.

Author contributions: A.C. designed the methodological approach and analyzed the data; P.L.P., E.T.P., and E.N.B. designed the experiments; P.L.P., E.T.P., J.L.W., A.F.S.-G., P.G.H., C.T.-S., K.H., and E.N.B conducted the experiments; and A.C. and E.N.B. wrote the paper.

The authors declare no conflict of interest.

This article is a PNAS Direct Submission. R.K. is a guest editor invited by the Editorial Board.

Freely available online through the PNAS open access option.

[1]To whom correspondence should be addressed. E-mail: aylin@nmr.mgh.harvard.edu.

This article contains supporting information online at www.pnas.org/lookup/suppl/doi:10.1073/pnas.1017041108/-/DCSupplemental.

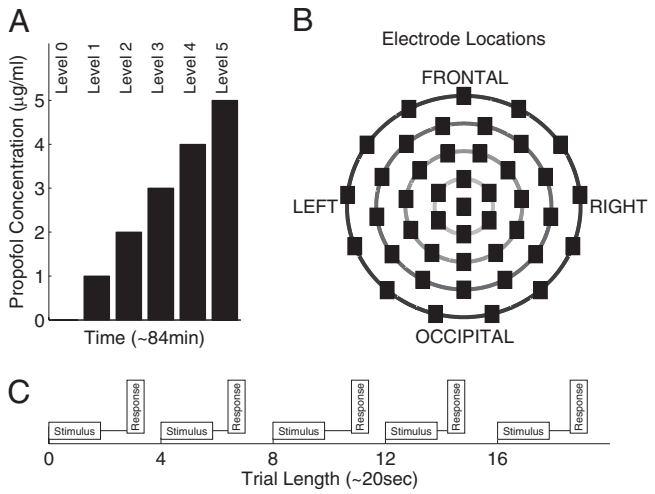

Fig. 1. Overview of the experiment. (*A*) Target effect-site concentrations of the anesthetic propofol delivered to each subject. (*B*) EEG electrode sites viewed from the top of the head. (*C*) Timeline of the auditory tasks, presented at 0, 4, 8, 12, and 16 s within each trial (*Materials and Methods*). Forty-two trials were presented per level.

Results

Sixty-four channels of EEG were measured as subjects executed a binary choice auditory task while receiving an increasing dose of the general anesthetic propofol delivered by a computer-controlled infusion (Fig. 1 *A* and *C*). We first analyzed the local EEG dynamics by computing the spectrograms of radial current density estimated by the surface Laplacian referencing at each of 44 of the 64 electrode sites (Fig. 1*B*). Next, we analyzed the network dynamics of the radial current density estimates by computing the cross-spectral matrix for each spectral frequency as a function of time. We summarized the temporal evolution of the spatial structure in the cross-spectral matrix by performing an eigenvalue decomposition at each frequency and computing the global coherence. At frequencies exhibiting high global coherence (i.e., those at which the leading eigenvalue was an appreciable fraction of the sum of the eigenvalues), we analyzed the spatial structure of the coordinated activity to determine which electrode sites contributed most to the global coherence.

Spectrograms of the Radial Current Densities Show Distinct Spatial Patterns. The spectra computed at the 44 sites at which the radial current densities were estimated (Fig. 1*B*) showed distinct changes in power (Fig. 2) as the subject received increasing doses (Fig. 1*A*) of propofol. Because the subject was lying awake with his eyes closed, the spectra showed the characteristic α activity pattern in the occipital sites (Fig. 2, occipital). As the dose of propofol was increased (Fig. 1*A*), changes in power occurred across the entire scalp. The α power decreased and δ power increased over the occipital sites. This was accompanied by a concomitant sharp, transient increase in β power (≈20 Hz) across all sites that was markedly more pronounced over the frontal sites. The increase in β power was followed by an increase in δ (0–4 Hz) power occurs at all sites and an increase in α power predominantly in the frontal sites (Movie S1). To show the importance of local referencing for tracking site-specific dynamics, we compared these spectra (Fig. 2) with ones computed from the same EEG recordings using an average referencing scheme (Fig. S1, same color scale as in Fig. 2). The spectra computed with respect to the average reference show an overall enhancement of power and the predominance at all sites of the dynamics (Fig. S1). This enhancement is seen only in the frontal sites in the locally referenced spectra (Fig. 2, frontal sites). As a consequence, at the high propofol doses (Fig. 1*A*) the decrease in the α power observed in the spectra computed over the occipital sites with local referencing (Fig. 2, occipital sites) was hidden by the widely distributed frontal power induced by the average referencing. The greater α and δ power in the frontal sites is still discernible.

Dynamics of the Occipital Power of the Radial Current Densities Relates to Behavior. In this experiment, loss of all responses to the auditory task defined the state of unconsciousness. We observe a clear correspondence between changes in spectra over the occipital sites and the behavioral responses (Fig. 3). The effect of propofol on the behavioral responses (Fig. 3, brown curves)

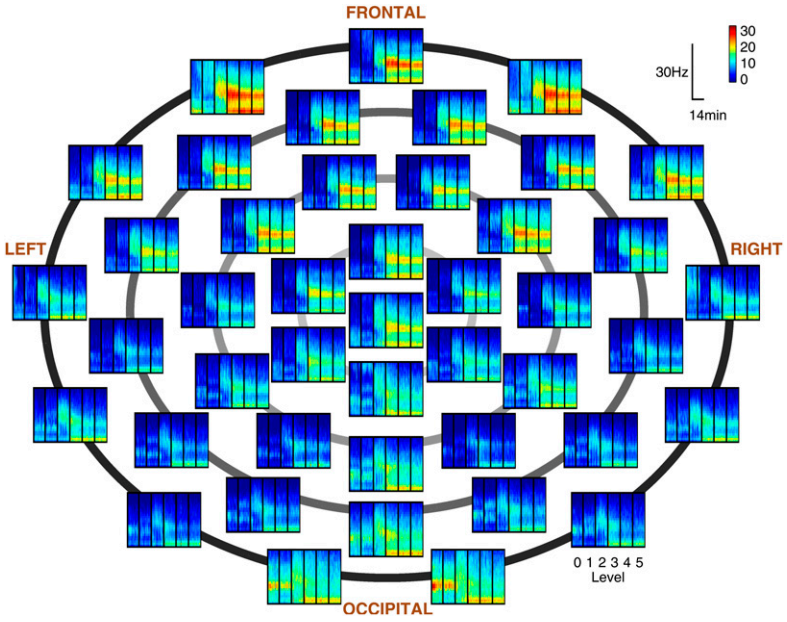

Fig. 2. Spectrograms of the radial current density estimated at the electrode sites in Fig. 1*B*. The five different propofol levels are demarcated by the black vertical lines in each spectrogram. *x* axis, time (0–~84 min); *y* axis, frequency (0–30 Hz).

differed among the subjects. In particular, subject 2 stopped responding over a short time window (Fig. 3*B*), whereas the other two subjects (Fig. 3 *A* and *C*) stopped responding over a wider time window. For all three subjects the dynamics of the power in the α range (Fig. 3, red curves) and in the δ range (Fig. 3, blue curve) from occipital sites (Fig. 3) showed a strong correspondence with the behavioral responses. Subjects showed a higher α power than δ power during periods in which they were awake, as identified by correct responses to the auditory task. As the number of correct responses decreased significantly, the ratio of the α and δ power approached 1. At the point when the α and δ power became approximately equal, the subjects no longer responded. After loss of consciousness, the δ power exceeded the α power for all subjects, and this relation became more pronounced as the dose of propofol continued to increase.

These changes in occipital α and δ power tracked even transient changes in the behavioral responses. To illustrate, at the point during level 2 when subject 3 (Fig. 3*C*) briefly stopped responding, the α power dropped below the δ power. The subject started responding again, and the α power exceeded the δ power. Subsequently during level 3, when subject 3 stopped responding the α power again dropped below the δ power and remained this way through level 5. During this period the subject remained unconscious. By contrast, the relationship between the α and δ power and the behavioral responses are obscured with average referencing. The occipital spectrograms computed using average referencing resembled the frontal spectrograms (Fig. S1).

Global Coherence Analysis Shows Strong Coordinated Activity in the α Range. The spectrograms showed that there were different spectral dynamics at different electrode sites as the dose of propofol was increased. To characterize the extent of coordinated activity across the electrode sites, we applied global coherence analysis (10). We analyzed the dynamics of the leading eigenvectors and eigenvalues of the cross-spectral matrix of the radial current density estimated at 44 sites on the scalp (Fig. 1*B*). For a given trial ℓ and frequency f, the i,j^{th} element of the cross-spectral matrix $C(\ell,f)$ is an estimate of the cross-spectrum between the radial current density estimate calculated at electrode sites i and j. The diagonal entries of this matrix contain the spectral power on trial ℓ at frequency f. As discussed in *Materials and Methods*, an eigenvalue decomposition of this matrix leads to a frequency-dependent set of eigenvectors. These eigenvectors are described entirely by their spectral power or equivalently, their eigenspectra. The degree to which the leading eigenvalue captures the dynamics can be quantified by the global coherence (10). For $N = 44$ electrode sites, global coherence at a given frequency is a number between $1/N = 0.023$ and 1, that is, the ratio of the largest eigenvalue of the cross-spectral matrix to the sum of the eigenvalues. The minimum value is attained when the readings from all electrode sites are random, whereas the maximum is attained when they are completely coherent. A large value of the global coherence suggests coordinated activity. The direction associated with the leading eigenvector explains a high fraction of the variance at the given frequency. Analyzing how much each site contributed to this eigenvector helps identify likely sources of the coordinated activity.

For each subject we computed the global coherence on each trial of the auditory task (*Materials and Methods*) at each spectral frequency and analyzed its dynamics as a function of dose of propofol (Fig. 4). During the awake state, subject 1 showed high global coherence (>0.6) in high α and β (12–30 Hz) ranges at level 0 and in the α range during level 1 (Fig. 4*A*). Subjects 2 and 3 showed a high global coherence only in the α range (Fig. 4 *B* and *C*). During his transient loss of consciousness during level 2, subject 3's high global coherence briefly vanished and recovered as the subject recovered consciousness. For all subjects, as the number of correct responses (Fig. 4, brown curve) decreased, global coherence became low. The level at which low global coherence was observed differed from subject to subject. Subjects 1 and 2 started to show strong global coherence values (>0.6) in the α range during level 3, whereas subject 3 showed strong global coherence at level 4. These results suggest highly coordinated activity in the α range when subjects were unconscious at the highest dose of propofol. In contrast, the strong δ oscillations observed at all sites when the subjects were unconscious do not show any coordinated activity.

To analyze which sites contributed most to the high global coherence, we focused on 11 Hz, the frequency in the α range at which the global coherence was the highest. Using the row weights from the weight matrix (*Materials and Methods*), Fig. 5 shows the contributions of each of the electrode sites to the leading eigenvector at 11 Hz when the subjects were awake and

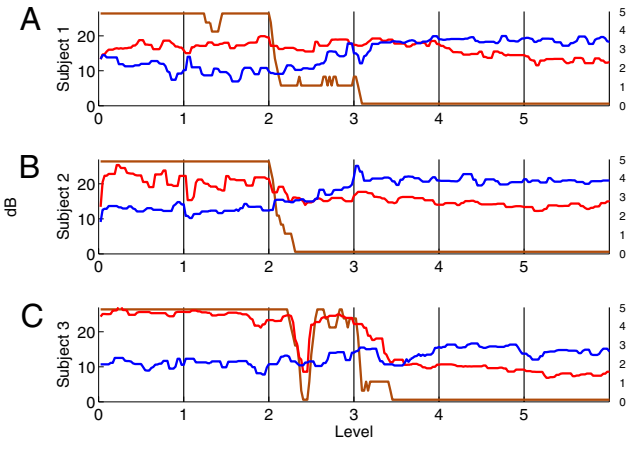

Fig. 3. (*A–C*) Behavioral curves computed as the number of correct responses from a possible 5 on each trial (brown curve, scale on the right), the average delta (0- to 4-Hz range) power (blue curve) and the average alpha (8- to 12-Hz range) power (red curve) per trial computed from the radial current density estimated at a single occipital site. Behavioral and power curves were smoothed with a median filter.

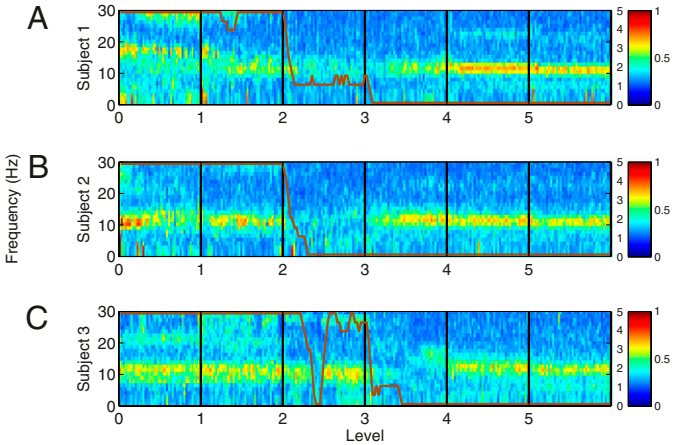

Fig. 4. (*A–C*) Time course of the global coherence computed at each frequency using the electrode sites in Fig. 1*B*. Global coherence values (color coded, scale on the right) close to 1 (red) suggest highly coordinated activity among the electrode sites whereas global coherence values close to 0 (blue) suggest an absence of coordinated activity. Global coherence values >0.6 (yellow–red) observed in the alpha range during the conscious state (levels 0 and 1) and during the unconsciousness (levels 4 and 5). The behavioral curve (brown) is defined in Fig. 3.

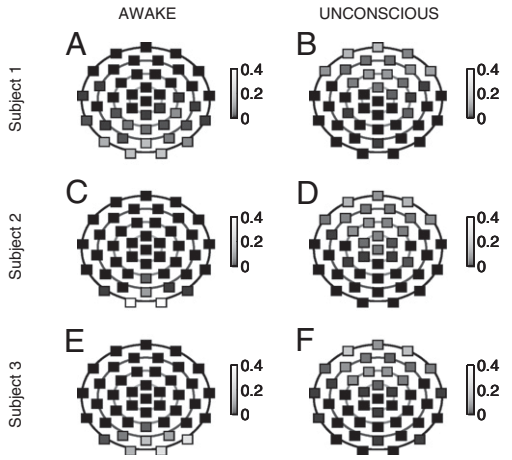

Fig. 5. Snapshots of the row weights for each electrode site (Fig. 1*B*) during high global coherence at 11 Hz. The row weights were high over the occipital sites when the subjects were awake (*A*, *C*, and *E*), level 1, and high over the frontal sites when the subjects were unconscious (*B*, *D*, and *F*), level 5. Color scale (0–0.4) for the row weights are on the right.

when the subjects were unconscious. The row weights sum to 1, and the larger the row weight the greater contribution of the corresponding electrode site to the leading eigenvector. For all subjects, the dominant contributions to the global coherence during the awake state came from the occipital sites, whereas during the unconscious state it came from the frontal sites. To evaluate further the differences in the contributions to global coherences between the awake and the unconscious states, we sorted the row weights in descending order and plotted at each trial the cumulative sum of the weights (Fig. 6), using a color scheme (Fig. 6, *Inset*) to make it easier to determine how the different electrode sites contributed to the leading eigenvector. Although the global coherence was high, both during the awake and unconscious states, there were clear differences in the sites contributing to the first eigenvector. In particular, a few occipital sites made up most of the contribution when the subjects were

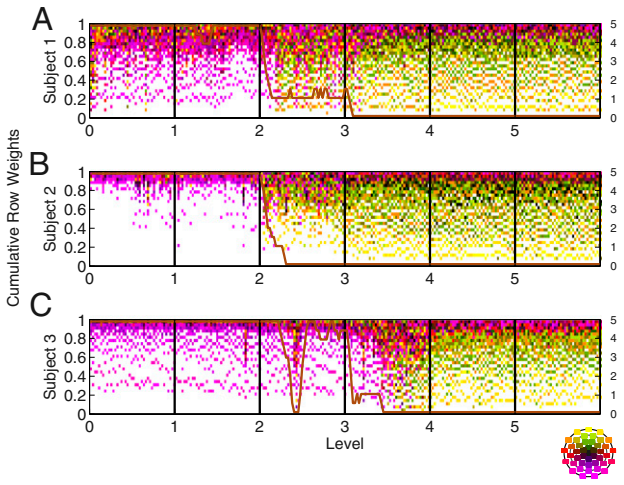

Fig. 6. (*A*–*C*) Time course of the cumulative sum of the row weights at each trial showing the contribution of each electrode site (Fig. 1*B*) to the leading eigenvector at 11 Hz. The row weights sum to 1 by definition. The color scheme identifies the spatial location of the electrode sites (*Inset*) with the occipital sites being colored pink-purple and the frontal sites being colored yellow-green. The color scheme has left–right symmetry. The behavioral curve (brown) is defined in Fig. 3.

awake (Fig. 6, levels 1 and 2). This is consistent with the fact that the α rhythm generated in the eyes-closed awake state was strongest in the occipital leads (Fig. 2). In contrast, several frontal sites were responsible for most of the contributions during the unconscious state (Fig. 6, levels in which the subjects did not respond). The relationship between the time course of the global coherence and the behavioral responses (Fig. 4) together with analysis of the composition of the first eigenvector (Fig. 6) show that the loss of a subject's ability to respond was closely related to the transition from coordinated activity concentrated over a small number of occipital sites to coordinated activity distributed over several frontal sites (Fig. 6). During the intermediate periods when both occipital and frontal sites contributed (Fig. 6), the observed global coherence was low for all subjects (Fig. 4). We verified the robustness of the global coherence estimates by computing a smoother cross-spectral estimate obtained by doubling the number of segments and averaging the estimates over a narrow band of frequencies. The results presented here are unaffected by these alternative estimates of the global coherence (Figs. S2 and S3).

We compared the global coherence (Fig. S4 *A*, *F*, and *K*) with other ratios of combinations of the first three eigenvalues of the cross-spectral matrix to the sum. The ratios of the second and third eigenvalues to the sum of the eigenvalues were small for all subjects for all levels (Fig. S4 *B*, *C*, *G*, *H*, *L*, and *M*). Not surprisingly, including these eigenvalues in our analysis either separately (Fig. S4 *D*, *I*, and *N*) or together (Fig. S4 *E*, *J*, and *O*) does not alter our findings.

Discussion

Characterizing brain dynamics using high-density EEG recordings is important for understanding the neurophysiology of general anesthesia and for developing more principled strategies for monitoring the brain states of patients having general anesthesia for invasive surgical and medical procedures (19). We have shown that the spatiotemporal dynamics of the brain under general anesthesia can be tracked by combining spectrogram and global coherence analyses.

Our paradigm began by using surface Laplacian referencing to estimate the radial current densities perpendicular to the scalp at each electrode site. From these current density estimates, we computed the spectrograms at each electrode site. The local referencing allowed us to demonstrate that there were distinct temporal patterns in the spectrogram at different electrode sites (Fig. 2). This is in contrast to an average or single electrode referencing scheme for this problem, which would lead to the erroneous conclusion that approximately the same temporal pattern was present in the spectrogram at each electrode site (Fig. S1). To characterize the coordinated activity in the EEG time-series, we performed an eigenvalue decomposition of the cross-spectral matrix at each spectral frequency as a function of time, and we computed the global coherence (Fig. 4). Finally, we used the weight matrix to analyze which electrode sites contributed most to the spatial structure in the coordinated activity suggested by the global coherence (Figs. 5 and 6).

Our spectrogram and global coherence analyses showed different spatiotemporal activity at different states of general anesthesia. When the subjects were awake, the spectrograms showed strong occipital α activity. This pattern of high α power over the occipital region was expected because the subjects kept their eyes closed (20). When the subjects were awake, the coordinated activity likewise was most prominent in the α range and was confined to the occipital sites. After loss of consciousness, the spectrograms showed a loss of α activity and an increase in δ activity in the occipital sites and strong α and δ activity in the frontal sites. Increased power in the α, β, and δ ranges in the frontal sites after loss of consciousness is the well-known pattern of anteriorization (3, 21). As subjects lost responsiveness to the

auditory task, the coordinated activity over the occipital sites in the α range diminished. When the subjects were unconscious, strong coordinated activity in the α range was observed broadly over the frontal electrode sites at the point when the spectrograms showed the anteriorization pattern. Despite the overall high δ activity in the spectrograms, coordinated activity was only observed in the α range. The relative power in the occipital α and δ ranges reliably tracked the subjects' behavioral responses. The occipital α power was greater than the δ power when the subjects were awake, and the reverse was true when the subjects were unconscious (Fig. 3). The strong global coherence in the α range suggests highly coordinated activity in the frontal electrode sites. Eigenvalue decompositions of cross-spectral matrices have been used to analyze EEG time-series (16–18); here we report the use of global coherence and weight matrices along with spectrograms to analyze brain states under general anesthesia.

Several extensions can be made to this analysis paradigm. First, greater spatial accuracy can be achieved by increasing the number of EEG electrodes from 64 to 128 or 256. Second, we computed the surface Laplacian by taking the difference between the voltage recorded at an electrode site and the average of the voltages recorded at the electrode sites in a local neighborhood. More accurate estimates of radial current density can be computed by increasing the number of electrodes and by using a spline-based approach that takes account of the curvature of the head in the neighborhood of each electrode site (22). Third, in the current analyses we have used global coherence as a data analysis procedure to characterize the spatiotemporal dynamics of the EEG across different states of general anesthesia. A key future analysis will be to characterize the statistical properties of this procedure so that it can be used not only for descriptive or exploratory data analyses but also for conducting formal statistical inferences. Fourth, although we conducted our analyses of the EEG recordings in the electrode or sensor space, an alternative approach would be to solve the inverse problem and perform source localization (23) to analyze the spatiotemporal dynamics at the locations in the brain.

Finally, these very preliminary data analyses suggest that brain activity under general anesthesia may be more highly structured than previously appreciated. Therefore, our analysis paradigm should be used in human studies to investigate the neurophysiological mechanisms underlying this structure (24). These methodological extensions and experimental analyses will be the topics of future reports.

Materials and Methods

Experiment: Physiological Recordings, Drug Administration, and Behavioral Recordings. The study was approved by the Human Research Committee at Massachusetts General Hospital. Every subject gave informed consent before starting the study. The details of the protocol are reported in *SI Materials and Methods*. Physiological recordings including heart rate, blood pressure, end tidal carbon dioxide, and oxygen saturation, along with 64 leads of EEG, were recorded from two healthy (Anesthesiology Physical Status I) male subjects and one healthy female subject while they received a computer-controlled infusion of the anesthetic propofol to reach five different targeted effect site levels. An auditory binary choice task was continually administered by computer control approximately every 4 s during the propofol infusion to assess level of consciousness. At each drug level the subjects had 42 trials. Each trial comprised a set of five binary choice tasks. The behavioral responses were tallied as the number of correct responses given out of five on each trial. Loss of consciousness was defined as the point at which the subject stopped responding to the auditory task.

EEG Recordings and Referencing. During the experiment, the scalp EEG was recorded at a sampling rate of 5,000 Hz. Fig. 1*B* overlays the EEG recording sites as viewed from the top of the head. This overlay is also used with color coding in Fig. 6 (*Inset*) to represent the corresponding recording sites. Recording sites that share the same azimuthal angle (0°, 23°, 46°, 69°, or 92°) are drawn on the same circle. Within each circle, electrode sites are drawn with their relative polar angles.

Analysis of scalp EEG depends critically on the choice of the reference electrode. Standard procedures of referencing in the EEG literature include the choice of a single reference electrode, average referencing, and bipolar referencing. In high-density recordings, the radial current density can be estimated from the surface Laplacian of the potential (8). This approach provides an alternative, physically motivated referencing scheme. The appropriateness of surface Laplacian approaches for computing coherence measures and their advantages over other referencing schemes are well documented (8, 12). We compute the surface Laplacian at each electrode site given in Fig. 1*B*. Denoting the voltage recorded at the i^{th} electrode relative to the reference electrode located close to the top of the head as $V_i(t)$, we estimated the surface Laplacian of $V_i(t)$ as:

$$J_i(t) \equiv V_i(t) - \frac{1}{M}\sum_{m=1}^{M} V_i^m(t), \qquad [1]$$

where $V_i^m(t)$ denotes the voltage recording at the m^{th} closest electrode to electrode i. Thus, the EEG recorded at a particular location was locally referenced to an average of the EEG recorded at the neighbors. This is similar to the Hjorth Laplacian (25). The choice of M depended on the nearest electrodes to i^{th} electrode and on their locations' symmetry with respect to i^{th} electrode. For the electrode on the top of the head, which had six symmetrically distributed nearest electrodes, M = 6. For the remaining electrodes it was possible to find four or five neighbors that are arranged in an approximately symmetric configuration. In this case, we choose M = 4 or 5, respectively. For the electrodes at the edge, for which such a symmetric configuration cannot be approximated, surface Laplacian was not calculated. Therefore, radial current density estimates were not made. The recordings from these electrodes have been used to estimate the radial current density at nearby electrode sites.

Spectral Analysis. For each trial, out of the five stimuli presented, four had a fixed duration of 2 s (*SI Text*). These 2-s periods were divided into 0.5 s long nonoverlapping segments and Fourier transform estimates of the surface Laplacians were computed at each electrode site. The data were first detrended by removing the best straight line fit to $J_i^k(t)$ from each segment k: $z_i^k(t) \equiv J_i^k(t) - (a_i^k t + b_i^k)$. The Fourier transform of $z_i^k(t)$ was computed as:

$$Z_i^k(f) = \sum_{t=0}^{N-1} z_i^k(t)u(t)e^{2\pi f\sqrt{-1}t}. \qquad [2]$$

Here, N is the number of samples in the window under consideration, and we have set the sampling interval to 1. The function, $u(t)$, is a windowing function chosen to be the first Slepian sequence. It is normalized so that $\sum_{t=0}^{N-1} u(t)^2 = 1$ as in ref. 26. We used custom-built Matlab scripts along with Chronux software (27) to compute the frequency domain quantities.

Spectrum. For each trial, the spectrum of the surface Laplacian at the location of the i^{th} electrode site is estimated by averaging over K nonoverlapping segments:

$$S_i^X(f) = \frac{1}{K}\sum_{k=1}^{K} X_i^k(f)X_i^k(f)^*, \qquad [3]$$

where $X_i^k(f) \equiv Z_i^k(f) - \frac{1}{K}\sum_{k=1}^{K} Z_i^k(f)$ is the mean corrected Fourier transform of the current density estimate at electrode site i of segment k at frequency f, and $X_i^k(f)^*$ is its complex conjugate. Because four fixed duration (2 s) stimulus periods were present in each trial, we obtained 16 nonoverlapping 0.5-s segments. We estimated the spectrum from at most 16 nonoverlapping 0.5-s segments. We omitted segments in which data showed artifacts, such as saturation of the range and abnormally sharp, high-amplitude changes. We included 96% of the segments in the analysis.

Cross-Spectral Matrix. Our method-of-moments estimate of the i, j^{th} element of the cross-spectral matrix at a frequency f was computed as:

$$C_{ij}^X(f) = \frac{1}{K}\sum_{k=1}^{K} X_i^k(f)X_j^k(f)^*, \qquad [4]$$

where $X_i^k(f)$, and $X_j^k(f)$ are the tapered Fourier transforms of the current density estimates from electrode sites i and j, respectively, at frequency f. For N locations, $C^X(f)$ is an $N \times N$ matrix of cross-spectra. In our case, N = 44

corresponds to the number of locations at which we computed current density estimates by using the surface Laplacian referencing (Fig. 1*B*).

Orthogonal Basis. We obtained an orthogonal basis by performing a Karhunen-Loève transform (28) at each frequency, *f*:

$$Y^k(f) = U(f)^H X^k(f), \quad [5]$$

where $U(f)^H$ is the adjoint of the matrix $U(f)$ [i.e., the complex conjugate transpose of $U(f)$, $U(f)^H = (U(f)^*)^T$] and a unitary matrix [i.e., $U(f)\ U(f)^H = 1$]. We chose $U(f)^H$ so that under the Karhunen-Loève transform the cross-spectral matrix in the new basis

$$C_{ij}^Y(f) = \frac{1}{K}\sum_{k=1}^{K} Y_i^k(f) Y_j^k(f)^* \quad [6]$$

is diagonal [i.e., $C_{ij}^Y(f) = C_{ii}^Y(f)\delta_{ij}$]. This implies that the diagonal elements of $C^Y(f)$ contain the eigenvalues of $C^X(f)$, and the columns of $U(f)$ contain the corresponding eigenvectors at frequency *f*. Specifically, the i^{th} eigenvalue is $C_{ii}^Y(f) = S_i^Y(f)$, where $S_i^Y(f) = \frac{1}{K}\sum_{k=1}^{K} Y_i(f) Y_i(f)^*$ is the power in the i^{th} eigenvector, and the i^{th} column of $U(f)$ is the normalized eigenvector satisfying $\sum_{j=1}^{N} |U_{ji}(f)|^2 = 1$. Therefore, $|U_{ji}(f)|^2$ contains the contribution from the j^{th} electrode to the i^{th} eigenvector. We term the matrix whose j^{th} and i^{th} element is $|U_{ji}(f)|^2$ the *weight matrix*.

Global Coherence. Sorting the eigenvalues, $S_1^Y(f) \geq S_2^Y(f) \geq \ldots \geq S_N^Y(f)$, the ratio of the largest eigenvalue to the sum of eigenvalues is:

$$C_{\text{Global}}(f) = \frac{S_1^Y(f)}{\sum_{i=1}^{N} S_i^Y(f)}. \quad [7]$$

This ratio is called the global coherence (10). When the leading eigenvalue is large compared with the remaining ones, $C_{\text{Global}}(f)$ is close to 1. In this case, examining the contributions of different sites to the corresponding eigenvector by using the elements of the weight matrix provides a summary of coordinated activity at this frequency. We refer to these elements as *row weights*. The row weights can be obtained by the absolute value square of the elements of the row of $U(f)^H$, which leads to the eigenvector with the highest eigenvalue.

ACKNOWLEDGMENTS. We thank Hemant S. Bokil and Nicholas D. Schiff for numerous conversations and suggestions. This work was supported by National Institutes of Health Grants DP1 OD003646 (to E.N.B.), DP2-OD006454 and K25-NS05758 (to P.L.P.), 2T32NS048005-06 (to P.G.H.), and General Clinical Research Center Grants 1 UL1 RR025758-01 and M01-RR-01066.

1. Gibbs F, Gibbs E, Lennox W (1937) Effect on the electroencephalogram of certain drugs which influence nervous activity. *Arch Intern Med* 60:154–166.
2. Kiersey DK, Bickford RG, Faulconer A, Jr. (1951) Electro-encephalographic patterns produced by thiopental sodium during surgical operations; description and classification. *Br J Anaesth* 23:141–152.
3. Tinker JH, Sharbrough FW, Michenfelder JD (1977) Anterior shift of the dominant EEG rhytham during anesthesia in the Java monkey: Correlation with anesthetic potency. *Anesthesiology* 46:252–259.
4. Kearse LA, Jr., Manberg P, Chamoun N, deBros F, Zaslavsky A (1994) Bispectral analysis of the electroencephalogram correlates with patient movement to skin incision during propofol/nitrous oxide anesthesia. *Anesthesiology* 81:1365–1370.
5. Billard V, Gambus PL, Chamoun N, Stanski DR, Shafer SL (1997) A comparison of spectral edge, delta power, and bispectral index as EEG measures of alfentanil, propofol, and midazolam drug effect. *Clin Pharmacol Ther* 61:45–58.
6. Rampil IJ, Kim JS, Lenhardt R, Negishi C, Sessler DI (1998) Bispectral EEG index during nitrous oxide administration. *Anesthesiology* 89:671–677.
7. John ER, et al. (2001) Invariant reversible QEEG effects of anesthetics. *Conscious Cogn* 10:165–183.
8. Nunez PL, Srinivasan R (2006) *Electric Fields of the Brain: The Neurophysics of EEG* (Oxford Univ Press, New York).
9. Rowan AJ, Tolunsky E (2003) *A Primer of EEG: With a Mini-Atlas* (Elsevier Science, Philedelphia).
10. Mitra P, Bokil H (2008) *Observed Brain Dynamics* (Oxford Univ Press, New York).
11. Jelles B, et al. (2008) Global dynamical analysis of the EEG in Alzheimer's disease: frequency-specific changes of functional interactions. *Clin Neurophysiol* 119:837–841.
12. Fein G, Raz J, Brown FF, Merrin EL (1988) Common reference coherence data are confounded by power and phase effects. *Electroencephalogr Clin Neurophysiol* 69: 581–584.
13. Mann ME, Park J (1994) Global-scale modes of surface temperature variability on interannual to century timescales. *J Geophys Res* 99(D12):819–833.
14. Prechtl JC, Cohen LB, Pesaran B, Mitra PP, Kleinfeld D (1997) Visual stimuli induce waves of electrical activity in turtle cortex. *Proc Natl Acad Sci USA* 94:7621–7626.
15. Mitra PP, Pesaran B (1999) Analysis of dynamic brain imaging data. *Biophys J* 76: 691–708.
16. Lagerlund TD, Sharbrough FW, Busacker NE (2004) Use of principal component analysis in the frequency domain for mapping electroencephalographic activities: Comparison with phase-encoded Fourier spectral analysis. *Brain Topogr* 17:73–84.
17. Ombao H, Von Sachs R, Guo W (2005) SLEX analysis of multivariate nonstationary time series. *J Am Stat Assoc* 100:519–531.
18. Ombao H, Ho M (2006) Time-dependent frequency domain principal components analysis of multichannel non-stationary signals. *Comput Stat Data Anal* 50:2339–2360.
19. Brown EN, Purdon PL, VanDort CL (2011) General anesthesia and altered states of arousal: a systems neuroscience analysis. *Annu Rev Neurosci*, 10.1146/annurev-neuro-060909-153200.
20. Brown EN, Lydic R, Schiff ND (2010) General anesthesia, sleep, and coma. *N Engl J Med* 363:2638–2650.
21. Feshchenko VA, Veselis RA, Reinsel RA (2004) Propofol-induced alpha rhythm. *Neuropsychobiology* 50:257–266.
22. Law SK, Nunez PL, Wijesinghe RS (1993) High-resolution EEG using spline generated surface Laplacians on spherical and ellipsoidal surfaces. *IEEE Trans Biomed Eng* 40: 145–153.
23. Molins A, Stufflebeam SM, Brown EN, Hämäläinen MS (2008) Quantification of the benefit from integrating MEG and EEG data in minimum l2-norm estimation. *Neuroimage* 42:1069–1077.
24. Ching S, Cimenser A, Purdon PL, Brown EN, Kopell NJ (2010) Thalamocortical model for a propofol-induced alpha-rhythm associated with loss of consciousness. *Proc Natl Acad Sci USA* 107:22665–22670.
25. Hjorth B (1975) An on-line transformation of EEG scalp potentials into orthogonal source derivations. *Electroencephalogr Clin Neurophysiol* 39:526–530.
26. Percival DB, Walden AT (1993) *Spectral Analysis for Physical Applications: Multitaper and Conventional Univariate Techniques* (Cambridge Univ Press, New York), p 583.
27. Bokil H, Andrews P, Kulkarni JE, Mehta S, Mitra PP (2010) Chronux: A platform for analyzing neural signals. *J Neurosci Methods* 192:146–151.
28. Jain AK (1989) *Fundamentals of Digital Image Processing* (Prentice Hall, Englewood Cliffs, NJ), p 569.